1 # Hydrocracking of complex mixtures: From bulk properties, over

2 # fundamental kinetics to detailed product composition

3 César G. Pernalete. P., Javier Ibáñez, Pedro S. F. Mendes, Kevin M. Van Geem, Joris W. Thybaut

4 *Ghent University, Laboratory for Chemical Technology (LCT). Department of Materials, Textiles and Chemical Engineering.*
5 *Technologiepark 125, 9052 Ghent, Belgium*

6

7 ## Abstract

8 Crude-Oil-to-Chemicals (COTC) is a novel concept in the oil industry in which the
9 production of base chemicals oil is preferred over fuels. This concept requires an
10 intensive integration of refinery and petrochemical operations and, in most cases,
11 hydroconversion and steam cracking play an essential role. In the present work,
12 particularly the role of hydroconversion is assessed in selected COTC scenarios via a
13 simulation framework based on fundamental modeling that seamlessly integrates a
14 Single-Event Microkinetics description of the cracking reactions with a molecular
15 reconstruction strategy based on Shannon Entropy maximization for determining the
16 detailed feedstock composition. Dealkylation and ring opening reactions have been
17 identified as the crucial ones to produce good steam cracker feeds, i.e., mixtures of
18 paraffins in the `C3-C21` range, especially n-paraffins. Simulation results show that for
19 a typical VGO paraffins yield in the desired fraction increases from 8.9% wt/wt to 19.6
20 % wt/wt with an increase of +5 kJ/mol in the acidity strength of the catalyst (ΔH_{prot})
21 and an increase of +10°C in the operation temperature. In general, it was found that
22 the yield of the total `C3-C21` fraction increased by +1.42 wt% per kJ/mol decrease of
23 the ΔH_{prot} of the catalyst, while per °C temperature increase the yield of the same
24 fraction increased by of +0.46 wt%.

25

26 **Keywords:** Single-event microkinetics, Complex mixtures, Molecular reconstruction,
27 Crude-Oil-to-Chemicals, simulation framework.
28
29

Corresponding author: `joris.thybaut@ugent.be` *(Joris W. Thybaut)*

## 1 Introduction

In a refinery, crude oils are generally converted for more than 90% to fuels. E.g., in 2019, the average conversion to fuel per oil barrel in the United Stated amounted to 93% [1]. Forecasts predict a decrease in the demand of fossil fuels in the coming decades [2]. This scenario pushes the oil industry to increase the production of other petroleum derivatives instead of fuels [3]. A traditional refinery would produce, at most, between 8% and 16% of naphtha's which can be subsequently converted to petrochemicals [4]. Further increasing the light products yield for processing in petrochemical plants requires significantly modified refining schemes [3].

The Crude Oil to Chemicals (COTC) concept refers to process configurations where more than 40% of the crude oil barrel is converted to chemicals in a single facility. A steam cracker typically plays a crucial role in this concept as a central element to produce ethylene and propylene [3, 5]. At present the virgin naphtha and the LPG from a refinery is often processed in steam crackers outside of the refinery complex [6]. In a COTC scheme the idea is to enhance the availability of light cuts that can be fed to an on-site fully integrated steam cracker [4]. For this purpose, mature catalytic conversion technologies such as Fluid Catalytic Cracking (FCC) and Hydroconversion (HDC), traditionally conceived to produce gasoline and diesel blends, are now configured as *feed preparation* units for a steam cracker [7]. In general, linear and iso-paraffins in a boiling range below 250°C ($\sim$ C3-C21) constitute the desired feed for steam cracking where high yields of ethylene and propylene can be produced [8].

In Figure 1 two potential COTC configurations are presented. Figure 1a shows a configuration in which middle distillates of a vacuum tower (Vacuum Gas Oil, VGO) are sent to a hydrocracker [7]. The light and medium cuts from the hydrocracker are blended with virgin light gases and liquids from the atmospheric distillation, as well as light fractions from deep conversion processes, to create a synthetic steam cracker feed.

An alternative configuration is shown in Figure 1b. It starts with a light crude oil (*CL*) that can be directly fed to a hydrocracker. The products of the hydrocracker are subsequently separated in an atmospheric distillation tower. The gas and liquid fractions are sent to the pool of intermediate products from which a blend will be produced and used as synthetic feed for the steam cracker. The bottom of the atmospheric distillation column is fed to a *Fluid Catalytic Cracking* (FCC) unit [4].

62 In both configurations the performance of the hydrocracker assumes a pivotal role. It
63 critically impacts on the molecular composition of the gaseous and liquids components
64 in the effluent that is sent to the blending pool. In addition, the hydrogenation level of
65 the heavy ends will determine the kind of units required for its further conversion [9,
66 10].

(a)

(b)

67
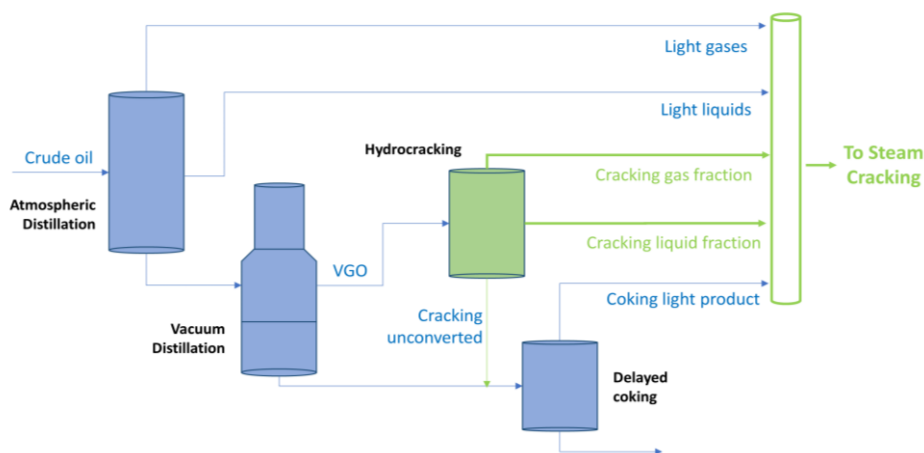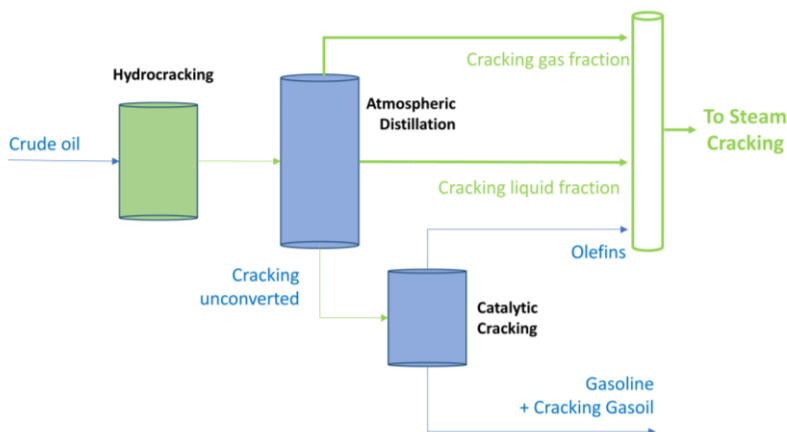
Figure 1.   Crude-Oil-To-Chemicals Process schemes: a) VGO as feed for
Hydrocracking [7], b) Full range crude oil as feed for Hydrocracking [4]

70 FCC and HDC are mature catalytic conversion technologies [6, 10, 11]. In a typical
71 refinery, the main purpose of FCC is to convert medium-heavy oil fractions towards
72 high octane molecules, mostly aromatics, that can be sent to the gasoline pool [12].
73 HDC is used to process similar feeds as FCC, the main goal being the production of
74 saturated molecules, such as iso-paraffines and naphthenes with high cetane index,
75 that can be sent to the diesel pool [10]. Several conventional ideas to optimize these

76 processes at a molecular level have been investigated in the past [12, 13, 14, 15].
77 However, the application of these processes as part of a scheme to primarily produce
78 feeds for steam crackers, as proposed in the Crude-Oil-to-Chemicals concept, results
79 in new challenges such as maximizing the production of base chemicals [4, 5, 7, 9].
80 Thus, despite the maturity of FCC and HDC, there is a window for optimization in the
81 context of the Crude-Oil-to-Chemicals process configuration. For this purpose, access
82 to detailed molecular compositions combined with fundamental microkinetic
83 modeling, allows to evaluate the behavior of mature processes under unusual operating
84 conditions or catalyst features, making this strategy crucial for a reliable design of such
85 configurations [16, 17].

86 The objective of this work is to make a fundamental analysis of the HDC unit in the
87 context of the COTC schemes described in Figure 1. Therefore, a Shannon based
88 feedstock reconstruction is employed for generating a molecular composition of heavy
89 feeds. This is integrated with a reaction kinetics based on elementary steps. The
90 resulting fundamental simulation program allows to identify the HDC catalyst and
91 corresponding operating conditions where high yields of valuable molecules that can
92 be used as feed for a steam cracker can be produced, within reach.

2   Models and methods

94 Hydroconversion (HDC) comprises two consecutive steps, i.e., hydrotreating (HDT)
95 and hydrocracking (HCK). The investigated process makes use of two reactors in series
96 where the feedstock is initially sent to a reactor with a high hydrogenation activity
97 catalyst. Subsequently, the effluent of this first reactor is fed to a second one with a bi-
98 functional catalyst that combines a hydrogenation and an acidic function required to
99 carry out the isomerization and cracking of the molecules.

100 Figure 2a schematically describes streams and reactors of the investigated process,
101 pointing out the typical available operational information for each of them. Figure 2b
102 depicts the conceptual abstraction used to simulate it, describing the key features of
103 each of the considered elements. An analogy is kept between the actual process and
104 the conceptual abstraction, which is used as a reference, as part of this work, to develop
105 a simulation framework to model hydroconversion processes. The framework allows to
106 describe the process streams at the molecular level embodying a kinetic model based

107   on elementary steps. This approach allows to acquire fundamental insights into the
108   HDC operation. Figure 2b schematically describes how the simulation framework
109   relate the bulk properties and the molecular representation of each stream, while using
110   a kinetic model based on elementary steps to simulate each reactor.
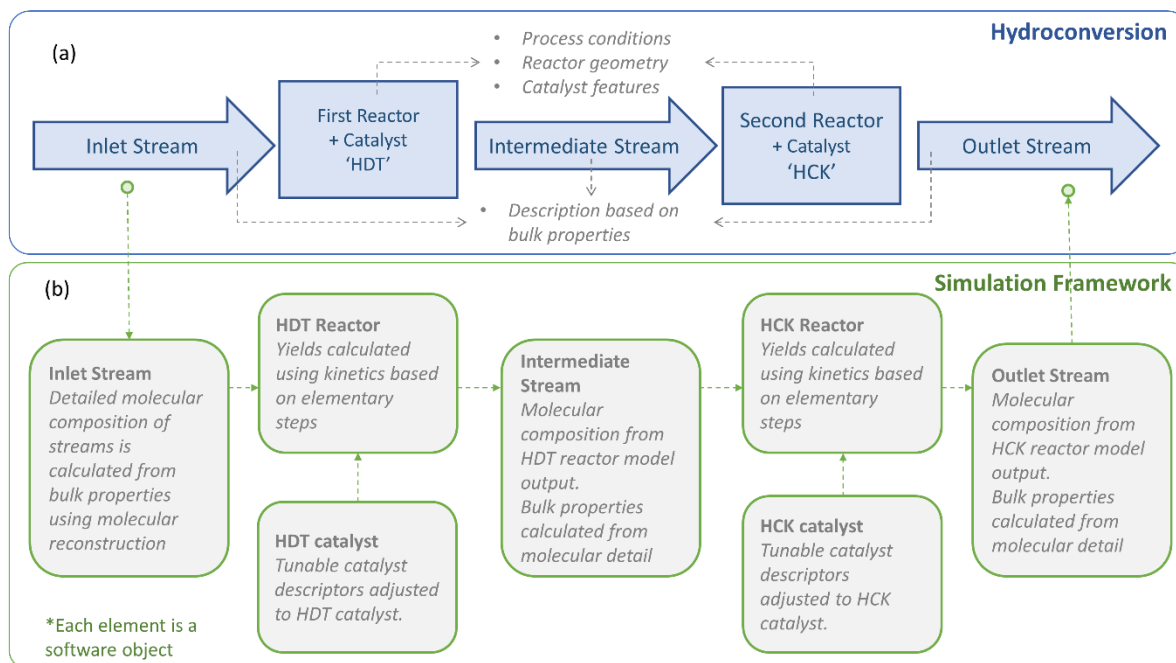
111

112   *Figure 2. (a) Schematic description of the process and (b) simulation framework*
113   *conceptual description*

2.1   Stream description

2.1.1   Shannon entropy based molecular reconstruction

116   The molecular composition of the complex hydrocarbon feed stream is obtained from
117   bulk properties via the so-called 'molecular reconstruction'. It was first reported by
118   Neurock and Klein [18, 19] who used a stochastic generation of molecular structures to
119   represent heavy oil fractions. The method applied in the present work follows an
120   alternative approach as was illustrated for naphtha and diesel fractions by IFPEN and
121   LCT [20, 21, 22]. Instead of regenerating the molecular library each time, a fixed
122   molecular library is used based on the detailed characterization of reference feeds,
123   while the composition is determined based on Shannon's theory of communication
124   [23]. The method consists of maximizing the Shannon Entropy given by Equation (1)
125   with x as the vector of mole fractions in the mixture. The solution of this maximization
126   problem ends up in the determination of the most probable components mole fractions

that meet the specified constraints. If only the mass balance constraint is given, the most probable composition is the equimolar one. If further constraints describing the properties of the mixture are given, as described in Equation (2), the method will find the statistically most probable composition that meets these constraints.

$$f(x) = \sum_{i=0}^{n} x \cdot lnx \quad \text{with} \quad \sum_{i=0}^{n} x = 1 \tag{1}$$

$$p_k - f_k(x) = 0 \quad \text{where} \quad k = 1, \dots, Np \tag{2}$$

Feed, intermediate and outlet streams composition as well as compound fractions along the reactor length are described with the same level of molecular detail. In case of intermediate streams and reactor content profiles, given the molar composition x, the calculation of each k bulk property from the molecular detail is made using the expresion $f_k(x)$ from Equation (2).

The molecular detail considered in this framework comprises ten (10) types of *lumps*, i.e., *Paraffins, Isoparaffins, (Mono to Tetra) -Naphthenes and (Mono to Tetra) - Aromatics* [24]. The considered carbon range for feed and products varies between C1 and C45. The considered experimental bulk properties p_k are specific gravity, composition by compound class (PNA: Paraffins, Naphthenes, Aromatics) and simulation distillated boiling point curve (ASTM D-2887) [25]. Additional experimental information, as more detailed family group composition or nuclear magnetic resonance studies determining hydrogen and carbon types, if available, could be used to make the calculated molecular description even closer to the real mixture [26, 27].

The use of molecular reconstruction in the context of hydrocarbon conversion is also reported by other authors [28, 29, 30]. The specific technique for heavier fractions employed in the present work [26] ensures a very elegant implementation of the optimization problem. An adequate linearization of the constraints and a Lagrange Multipliers approach is used to solve this non-convex optimization problem at very low computational cost [21].

2.1.2 Molecular representation of the feeds

Four different hydrocarbon mixtures were used in the study, three (3) Vacuum Gas Oils (VGO_A, VGO_B, VGO_C) and one (1) Light Crude Oil (CL). All feeds are characterized by

density, composition by compound class (Saturates, Mono-aromatics, Diaromatics, Triaromatics and Tetra-aromatics) and simulated distillation (ASTM D-2887). Using these *bulk* properties a detailed molecular description of the feed is determined by applying the methodology described in Section 2.1.1.


(a)

(b)
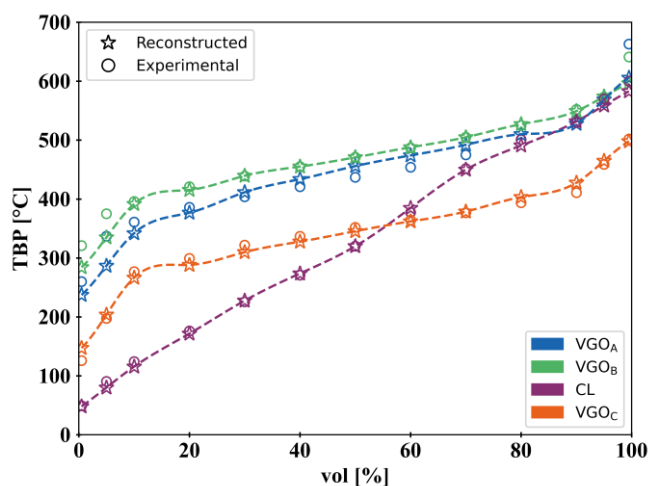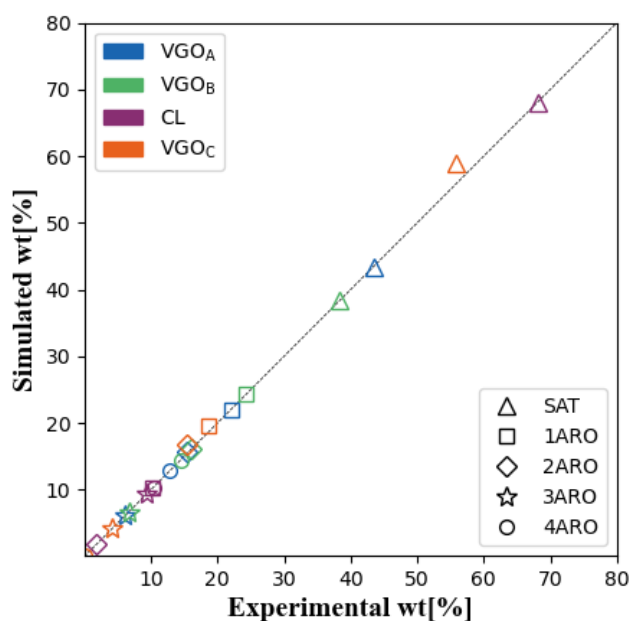
Figure 3. Experimental vs. reconstructed: (a) simulated distillation ASTM D-2887 and (b) composition by compound class

The experimental vs. reconstructed simulated distillation ASTM D-2887 as well as composition by compound class are depicted in Figure 3. From Figure 3a it can be

169   observed that VGO_A and VGO_B have higher Initial and Final Boiling Points than VGO_C.
170   These values allow to identify them as heavier fractions than VGO_C. In case of CL, the
171   Final Boiling Point is closer to the ones determined for VGO_A and VGO_B, but the Initial
172   Boiling Point is even lower than the one determined for VGO_C. These values indicate
173   that this hydrocarbon mixture comprises a high diversity of light and heavy molecules
174   which, according to Figure 3b, an important amount of them are saturated compounds.

175   A very good agreement between the reconstructed feedstocks bulk properties and
176   experimental data can be observed. Note that slight difference was found in the Final
177   Boiling Point for VGO_A and VGO_B shown in Figure 3a due to their high Final Boiling
178   Point (>600°C) and the use of a molecular library with compounds up to 45 carbon
179   atoms only. Note that the accuracy of the initial and final boiling point is known to be
180   lower than of the other boiling points [26]. In addition, given the special interest in the
181   lightest fractions, this mismatch is not expected to have an important effect in the
182   quantitative analysis presented in the upcoming sections. Figure 3b shows the very
183   good agreement between the experimental vs. reconstructed composition by
184   compound class for all feeds.

185   ## 2.2 Kinetics

186   ### 2.2.1 Single-Event MicroKinetics model

187   The origin of the fundamental kinetic modelling of hydrocracking and
188   hydroisomerization according to the single-event principle dates back to the early 80's
189   of the last century [31, 32]. The key idea is that each elementary step is accounted for
190   and, hence, all reaction intermediates are considered. Automated reaction network
191   generation methodologies were developed to assess all possible reactions that can take
192   place in hydroisomerization and hydrocracking of hydrocarbons [33, 34].

193   The single-event concept is based on transition state theory (TST). According to TST
194   the transformation of a reactant into a product via an intermediate activated complex
195   can be quantified via the following rate coefficient:

196
$$k = \frac{k_b \cdot T}{h} exp\left(\frac{\Delta S^{0,\#}}{R}\right) exp\left(-\frac{\Delta H^{0,\#}}{R \cdot T}\right) \tag{3}$$

197   Where $\Delta S^{0,\#}$ and $\Delta H^{0,\#}$ represent the activation entropy and enthalpy respectively [13].

198 In case the reaction mixture has a complex composition, the number of elementary
199 steps interconverting these compounds is very high. As a reference, according to
200 Martens and Marin [24] the hydrocracking network of only n-nonane comprises
201 already 44 alkanes, 175 alkenes and 138 carbenium ions that are interconverted by 182
202 alkyl shifts, 272 PCP branching reactions and 53 β-scissions, while for n-nonadecane
203 these numbers increase to 1981 alkanes, 25,065 alkenes and 20,437 carbenium ions
204 and 12,470 alkyl shifts, 15,970 PCP branching, and 6429 β-scissions. The complexity
205 for mixtures involving even heavier molecules is evident. If different kinetic parameters
206 would be determined for each of these reactions, this would be an insurmountable task.

207 This issue was successfully addressed by the development of the Single-Event
208 Microkinetics (SEMK) approach [35, 36, 37] as employed in the present work. In this
209 approach, the reaction rate is considered to be primarily determined by two features:
210 the reaction family depending on the type of carbenium ion involved *(s, t)*, and the
211 global symmetry of the molecule. To each reaction family, a unique rate coefficient is
212 attributed. As described in Equation (4), the impact of the global symmetry on the
213 reaction rate of each elementary step can be taken into account by expressing an
214 elementary step as the number of "single events", the latter being defined as the ratio
215 of the global symmetry numbers of reactant and activated complex [16, 38, 39, 40].
216 This way, it is possible to drastically reduce the required number of single-event rate
217 coefficients while preserving the fundamental nature of the model.

218
$$k = \frac{\sigma_{global}^{reactant}}{\sigma_{global}^{\#}} \cdot \tilde{k} = n_e \cdot \tilde{k} \tag{4}$$

219 In a SEMK model, the reaction rate of the acid catalyzed reactions, i.e., the rate-
220 determining steps under ideal hydrocracking conditions, are expressed as first order in
221 the alkyl carbenium ion concentration on the acid sites as follows [39]:

222
$$r^{\overline{crack}}^{iso}(m_{i,k}; n_{q,r}) = n_e \tilde{k}^{\overline{crack}}^{iso}(m_{i,k}; m_{q,r}) C_{R_{i,k}^+} \tag{5}$$

223 Various references can be found in literature of the application of the SEMK
224 methodology to hydrocracking [41, 42, 43, 44, 45, 46, 47, 48]. The SEMK model applied
225 here was developed for ideal hydrocracking on classical bifunctional catalysts
226 containing both a hydrogenation and an acid function [17]. The elementary acid
227 catalyzed reaction families considered in the hydrocracking of paraffinic compounds

228 are: (de)protonation, PCP branching, alkyl-shift and β-scission while the reactions
229 considered for naphthenic components are (de)protonation, intra ring alkyl shift, PCP
230 branching, PCP contraction, endocyclic β-scission and exocyclic β-scission.
231 Accounting for this limited number of families, an entire reaction network of
232 elementary steps can be simulated.

233 In order to guarantee the applicability of the model towards complex mixtures typically
234 involved in hydrocracking of real feeds, a specific version of the Single-Event
235 Microkinetics methodology, denoted as Relumped Single-Event Microkinetics
236 (RSEMK) [24], has been developed. In the RSEMK an 'a posteriori' lumping strategy
237 is applied with feeds originally characterized in terms of bulk properties and,
238 subsequently, reconstructed in terms of the considered lumps [42, 49]. In this strategy
239 the single-event rate coefficients for each reaction type are preserved and combined
240 with the so-called lumping coefficients [13]. Equation (6) shows the reaction rate
241 between the lump g and the lump h, where $LC(g,h)$ is the so-called lumping coefficient,
242 $\tilde{k}$ the single-event rate coefficient, $\widetilde{K}_{prot}$ the single-event protonation equilibrium
243 coefficient, C_t the total number of acid sites, $H_{L,g}$ the Henry coefficient of lump g for the
244 Langmuir physisorption K_L, p_i the partial pressure of lump i and $K_{L,f}$ the Langmuir
245 physisorption coefficient of lump f. Differences in hydrocracking performance
246 between two catalysts are attributed to differences in physisorption stabilization (K_L),
247 in acid site strength (ΔH_{prot}), and in capacity for physisorbed and chemisorbed species
248 (C_{sat} and C_{acid}, respectively). These parameters purely reflect the catalyst structure and
249 are denoted as "catalyst descriptors" [14].

$$r(g,h) = \frac{LC(g,h)k \cdot \widetilde{K}_{prot} \cdot C_t \cdot H_{L,g} \cdot p_g}{\left(1 + \sum_f K_{L,f}\, p_f\right)p_{H_2}} \tag{6}$$

251 A RSEMK model preserves the molecular detail of the Single-Event MicroKinetic
252 (SEMK) model but replaces the time consuming evaluation of the net production rates
253 of the individual species related to the large reaction networks involved in
254 hydrocracking [24, 42].

255 Later, hydrogenation of aromatics was also included in the model [50, 51]. Aromatic
256 hydrogenation modeling follows an approach analogous to the Horiuti Polanyi
257 mechanism as developed earlier. The model considers competitive adsorption of
258 dissociated hydrogen and aromatic species on the catalyst surface, followed by

successive reversible hydrogenation of the aromatic molecules. The addition of the third or the fourth H atom in the aromatic ring could be considered as rate determining; the resulting kinetic expression for any aromatic species being:

$$r_A = \frac{C_t \cdot k_i \cdot \left(\prod_{j=1}^{i} K_j\right) \cdot K_A \cdot K_{H_2}^{\ 2} \cdot C_A \cdot C_{H_2}^{\ 2}}{\left(1 + K_A \cdot C_A + \sqrt{K_{H_2} \cdot C_{H_2}}\right)} \qquad (i = 3,4) \qquad (7)$$

Where K_j is the equilibrium coefficient of ith H atom addition, k_i is the forward reaction rate of the rate-determining step, K_A and K_{H_2} are the chemisorption equilibrium coefficients for aromatic species and hydrogen respectively, C_t is the total concentration of active sites, C_A the concentration of each aromatic specie in the liquid phase and C_{H_2} the hydrogen concentration in the liquid phase. In the present work the addition of the fourth H atom is assumed as rate determining which, according to the conclusions of Thybaut et.al [50], is expected to better describe these reactions.

The above discussed kinetics is implemented in a one dimensional adiabatic heterogeneous plug flow reactor model including the following considerations: vapor-liquid equilibrium in the bulk gas-liquid interphase, catalyst surface completely covered by a liquid layer, internal mass transport effects inside the catalyst pellets and isothermal character within the catalyst particle as well as between the catalyst and the liquid phase. Internal mass transport limitations were considered by the calculation of effectiveness factors obtained by the integration of the simultaneous reaction and diffusion equations along the catalyst particle diameter. Details of the reactor model can be found in previous works [35, 24, 41, 40, 43, 52].

2.2.2 Catalyst descriptors

The single-event microkinetic model described in the previous section is fine-tuned by adjusting selected catalyst descriptors. Each reactor makes use of a different catalyst and, therefore, is described by a different set of catalyst descriptors. The tunable catalyst descriptors considered in the present work are the activation energy E_a for the hydrogenation reactions, that regulates the aromatics and alkenes hydrogenation activity, and the protonation enthalpy ΔH_{prot}, which accounts for the general "acid activity".

2.3 Simulation framework

2.3.1 Implementation details

The conceptual simulation framework illustrated in Figure 2 is coded using an object-oriented architecture [53, 54, 55] in Python 3 [56]. Three *classes* of *objects* are used: `stream`, `reactor` and `catalyst`. Multiple *objects* belonging to each *class* can be created simultaneously by setting its configuration parameters (*attributes*). Thus, three streams (3), two (2) reactors, and (2) catalyst are created to model the investigated process. During the configuration, each catalyst is linked to a different reactor. In a similar way, reactors and streams are configured to be linked according to the process flow sequence.

The *class* `Stream` contains two key functions (*methods*): one to define the 'molecular' composition of the stream departing from the bulk properties and the other to calculate the bulk properties from the 'molecular' detail of the stream. For this purpose the methodology described in Section 2.1.1 is applied. The *class* `Reactor` contains a key function for calculating yields and reactor content and temperature profiles using the RSEMK methodology described in Section 2.2.1.

Using this approach it is possible account for the 'molecular' detail. In addition, the strategy offers flexibility to evaluate multiple process configurations and explore the results without additional coding effort.

2.3.2 Simulation procedure

Initially, the reactor model is *fine-tuned* by adjusting the catalyst descriptors described in section 2.2.2 for every reactor until the simulated bulk properties match the experimental results for intermediate and final streams in the investigated process.

Fine tuning is based on the minimization of the difference between predicted and experimental bulk properties at the outlet of each reactor for specific experimental runs. The experimental data used for *fine tuning* was obtained at pilot scale using VGO_A and VGO_B as feeds. More specifically, isothermal tubular reactors were used in both steps with a Liquid Hourly Space Velocity $(LHSV) = 1.33 \; \frac{\frac{m^3}{h}}{m^3}, \; \frac{H_2}{HC} \; ratio = 850 \; \frac{Nm^3}{m^3},$ $Temperature = 660K$ and $Pressure = 13.1 \; MPa.$

The experimental vs. simulated composition by compound class after *fine tuning* are shown in Figure 4. In addition, the experimental vs. simulated ASTM D-2887 distillation curve of the intermediate and final streams can be observed in Figure 5. These values show a successful *fine tuning* of the kinetic model which is used to perform specific simulation studies described in the following section.

The first Case Study entails the processing of the feeds VGO_C and CL described in Section 2.1.2. The processing of VGO_C describes a hydroconversion scenario according to the scheme 'a' of Figure 1 while the processing of a Light Crude Oil describes an scenario according to the scheme 'b' of the same figure. The second Case Study, described in section 3.2, covers a set of simulations for a range of values in the protonation enthalpy and the process temperature. The purpose of this Case Study is to evaluate the effect of different operating conditions and catalyst features on the yield of compounds with carbon number in the range of `C3-C21`.

(a)   (b)
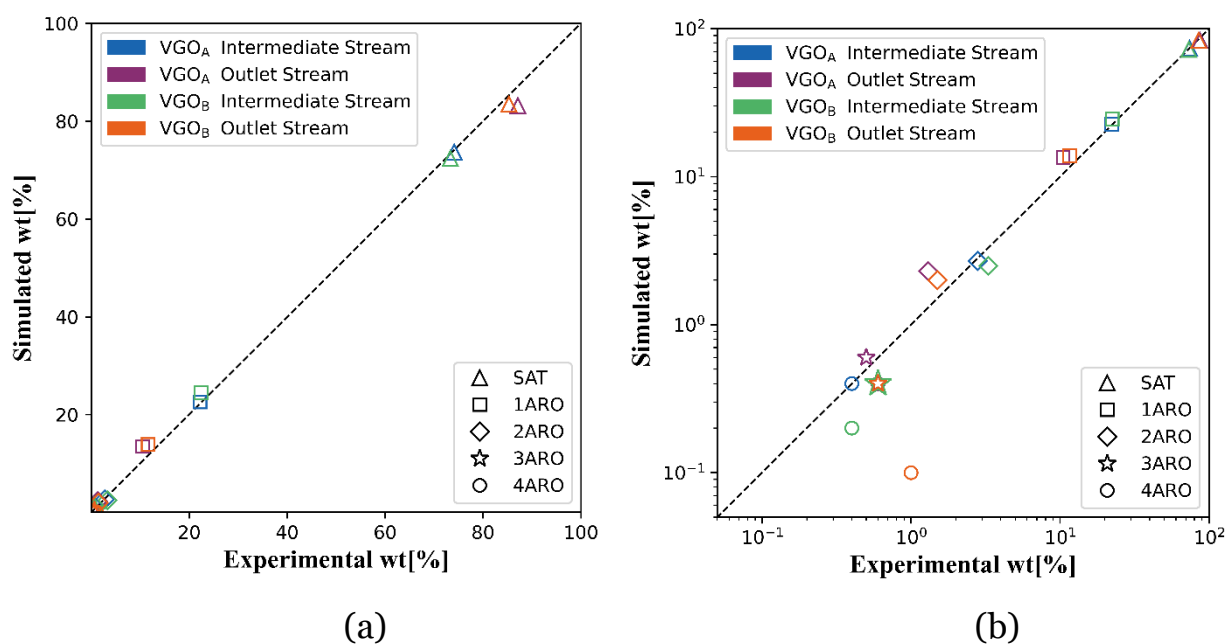
Figure 4. Experimental vs. Simulated composition by compound class for intermediate and outlet streams for VGO_A and VGO_B, a) Linear and b) Logarithmic

The applied simulation procedure is based on the generalization capabilities gained when using a fundamental description of the kinetics as described in Section 2.2.1. In addition, it relies on the versatility for feed characterization, at the molecular level, ensured by the Molecular Reconstruction methodology described in Section 2.1.1.

336 Since the catalyst descriptors are related to the nature of the catalytic function and are
337 independent of the feed being processed, the same catalyst descriptors can be used to
338 simulate processing of different feedstocks at varying operating conditions.
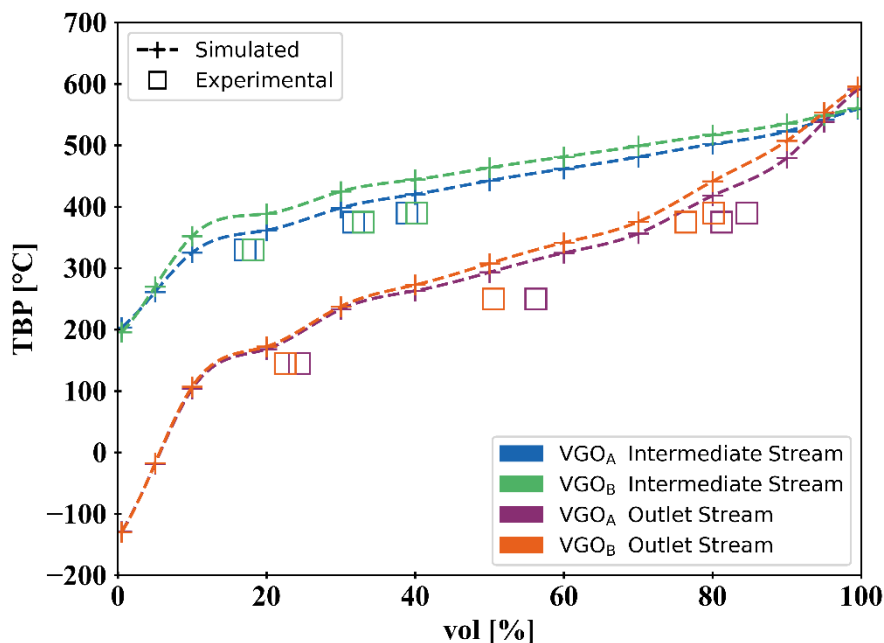
339

Figure 5. Experimental vs. Simulated ASTM D-2887 for intermediate and outlet
streams for VGO_A and VGO_B

3 Simulation: From hydrocracking toward chemicals

3.1 *Case Study*: Evaluating COTC scenarios

353 The hydroconversion process in the context of the Crude-Oil-To-Chemicals schemes
354 presented in Figure 1 are simulated using representative feedstocks for each case. For
355 the scheme presented in Figure 1a the Vacuum Gas Oil labeled as VGO_C is used, while
356 for the scheme of Figure 1b the processing of the full range crude oil labeled as CL is
357 simulated.

358 Since the developed framework allows to have available 'molecular' details of streams
359 and reactor content profiles, it is possible to acquire different insights in both
360 processes. Thus, the simulations results are presented in three ways: reactor content
361 profiles per boiling fraction (or "cuts"), reactor content profiles per mole fraction of
362 compound class and detailed molecular description of the streams per compound class
363 and carbon number.

364   The simulated reactor content profiles, for both cases VGO_C and CL, in terms of the

365   typical industrial refinery cuts i.e.; light hydrocarbons (< T_65), Naphtha (T_65_150),

366   Diesel (T_150_250), Light Vacuum Gas Oil (LVGO) (T_250_375), Heavy Vacuum Gas Oil

367   (HVGO) (T_T375_540) and residue (T_540_plus), are shown in Figure 6. Figures 6a and

368   6b represent the profiles for the VGO_C, while Figures 6c and 6d describe the profiles for

369   the Light Crude Oil (CL).
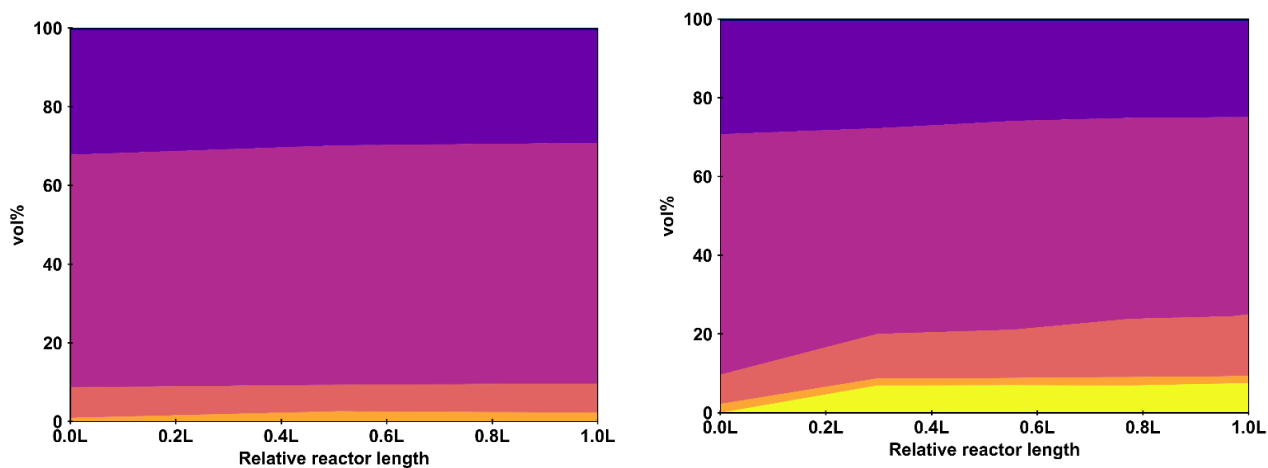
370

371   *(a) HDT reactor content profile for VGO_C*   *(b) HCK reactor content profile for VGO_C*
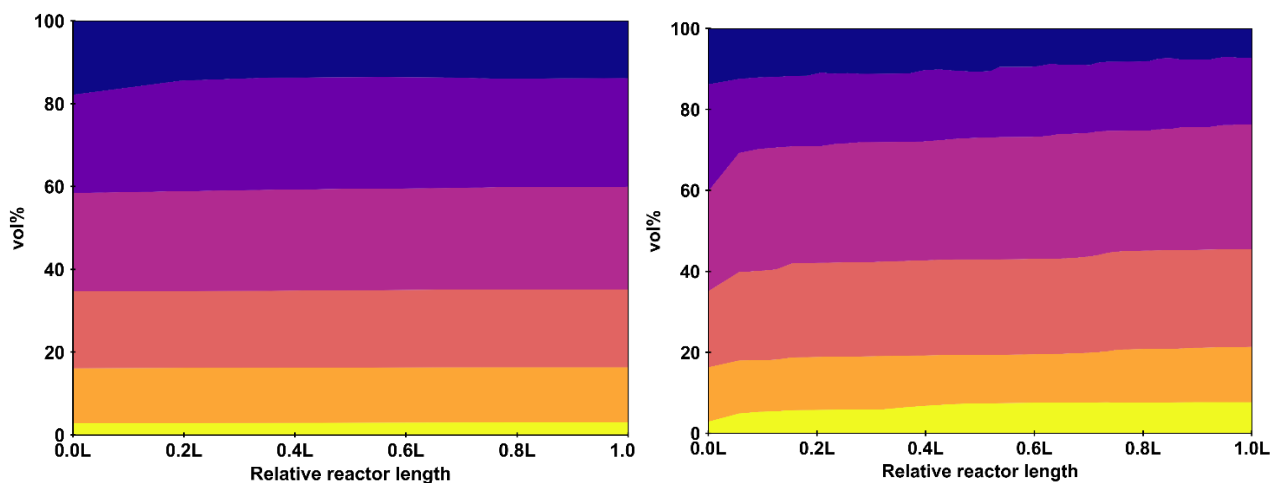
372   *(c) HDT reactor content profile for CL*   *(d) HCK reactor content profile for CL*

T_65	T_150_250	T_375_540
T_65_150	T_250_375	T_540_plus
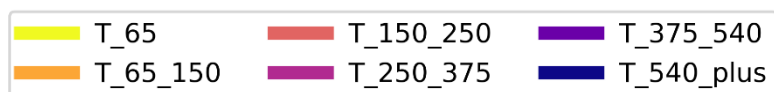
373

Figure 1. Hydrotreating (HDT) and Hydrocracking (HCK) reactor content profiles
for VGO_C and CL expressed in cuts based on boiling range

374 In both cases only very limited changes are obtained in the profile by boiling cuts in the
375 first stage as shown in Figures 6a and 6c due to low cracking activity in this reactor.
376 More pronounced changes are seen, for both cases, in the second reactor as evident
377 from Figures 6c and 6d.
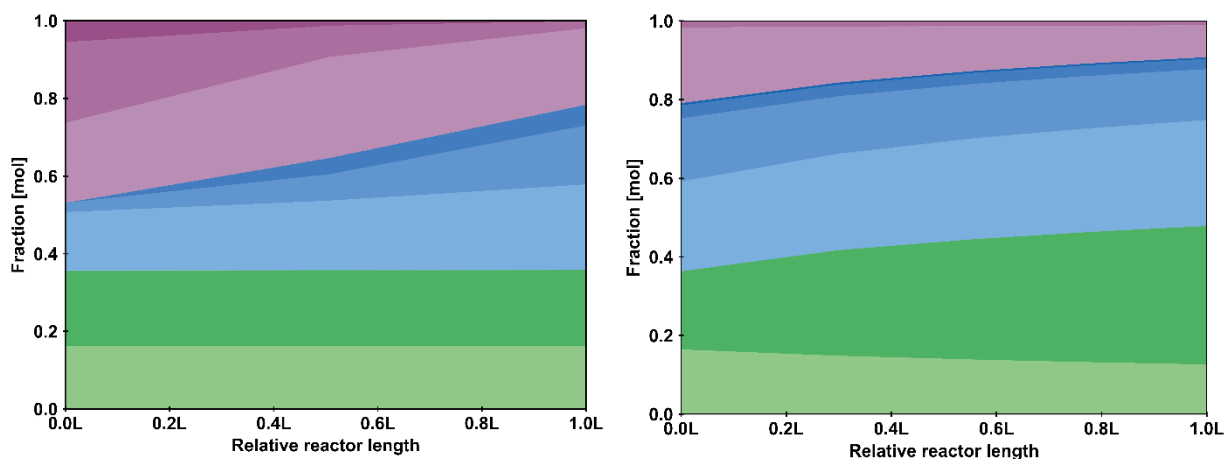
378

379 *(a) HDT reactor content profile for VGO_c*   *(b) HCK reactor content profile for VGO_c*
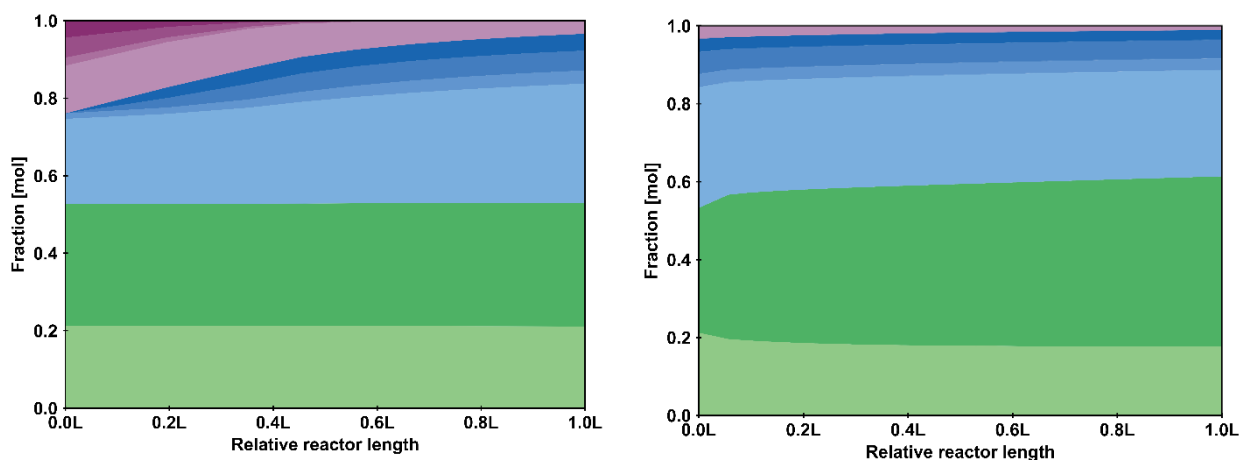
380

381 *(c) HDT reactor content profile for CL*   *(d) HCK reactor content profile for CL*
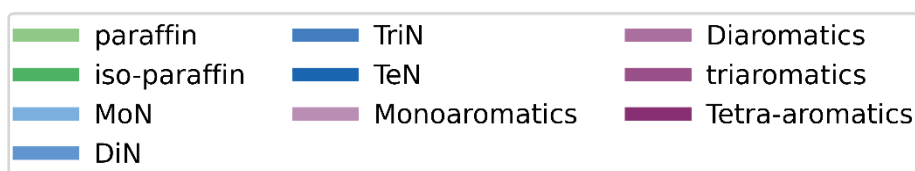
382

*Figure 2. Hydrotreating (HDT) and Hydrocracking (HCK) reactor content
profiles expressed in molar fraction per compound class*

383 Simulation results, for both cases, in terms of profiles per compound class are shown
384 in Figure 7. A decrease of 45% mol/mol in the total aromatic content of VGO_C, with
385 total hydrogenation of triaromatics, high level of hydrogenation of diaromatics and
386 relatively constant molar fraction of monoaromatics, is observed on Figure 7a. Figure
387 7c shows a decrease of 78% in the total aromatic content of CL, with a complete
388 hydrogenation of aromatics composed by more than one ring and a decrease of 42%
389 mol/mol in monoaromatics. Despite the presence of tetra-aromatics, the lower initial
390 total aromatic content in CL allows to reach higher levels of hydrogenation than VGO_C.
391 The corresponding production of naphthenes is observed in both cases. Figures 7b and
392 7d, exhibit further decrease of aromatics and n-paraffins concentration and increase of
393 iso-paraffins and naphthenes content. The hydrogenation activity also present in the
394 hydrocracking catalyst explains the further decrease in the aromatic content. The
395 increase of iso-paraffins and decrease of n-paraffins could be attributed to the rapid
396 isomerization of n-paraffins to iso-paraffins via methyl-shift and PCP branching,
397 possibly followed by β-scission when favorable configurations are formed [13, 57]. The
398 exocyclic β-scission of side branches in mono and multi-ring naphthenic also
399 contributes to the formation of iso-paraffins. Even though endocyclic β-scission of
400 naphthenes might also produce iso-paraffins the rate of this reaction is much slower
401 [52, 57].

402 The detailed molecular description of the inlet, intermediate and outlet stream, for
403 both cases, is shown in Figure 8. Figures 8a and 8b show the description of the feeds,
404 Figures 8c and 8d describe the intermediate streams and Figures 8e and 8f show the
405 outlet of the second reactor (HCK). The availability of the 'molecular' detail of the
406 streams allows to have a detailed insight in the chemistry that is taking place in the
407 process and further explain the phenomena observed in Figure 6 and Figure 7.

408 The analysis of the products in terms of typical industrial refinery cuts is made in the
409 following subsections.

410
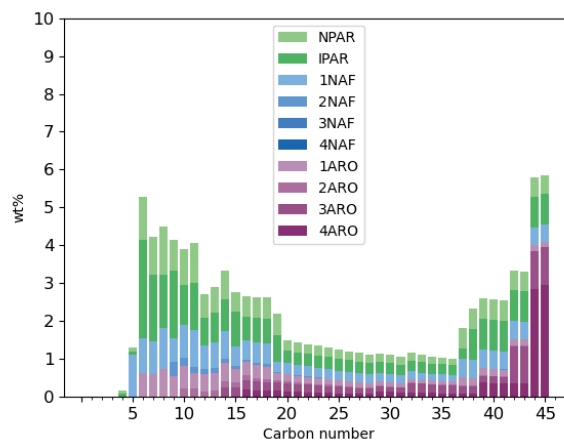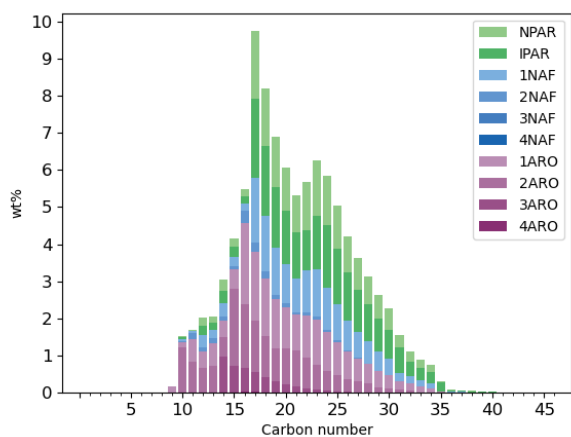
411   (a) VGO_C: Fresh feed   (b) CL: Fresh feed
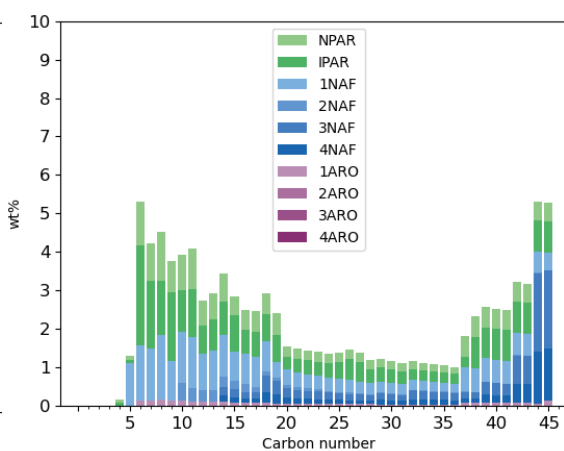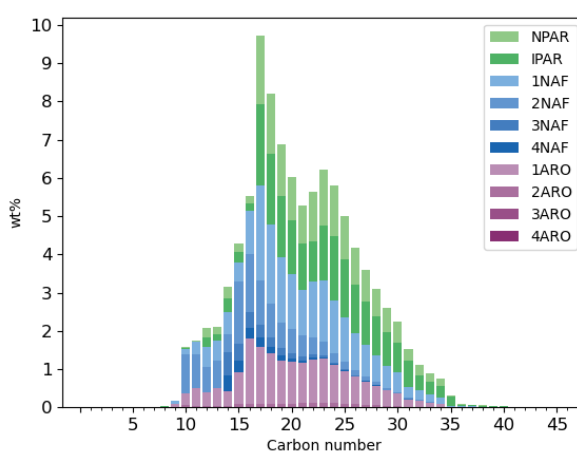
412   (c) VGO_C: HDT effluent   (d) CL: HDT effluent
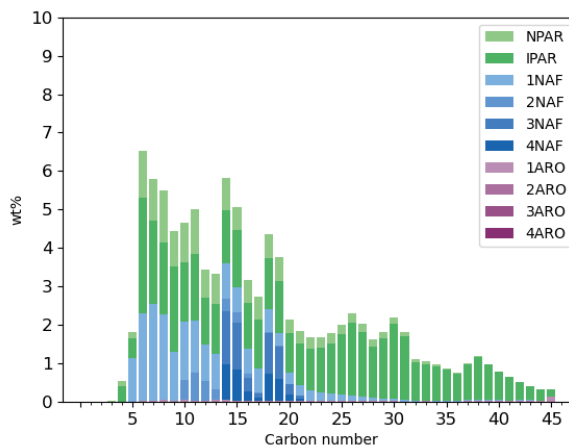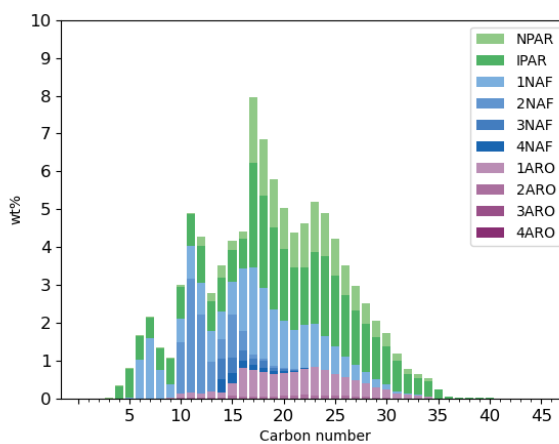
413   (e) VGO_C: HCK effluent   (f) CL: HCK effluent

414

415   *Figure 3. Molecular description of inlet, intermediate and outlet streams by compound class and carbon number*

416
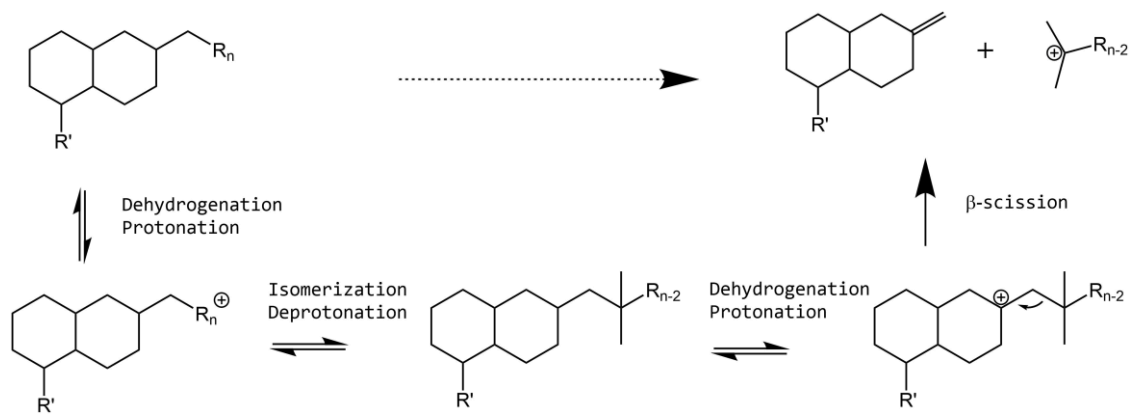
Figure 9. Exocyclic β-scission of di-naphthenes

3.1.1 Light hydrocarbons (< T_65) and Naphtha (T_65_150)

From Figure 6b and Figure 6d a rapid increase followed by stabilization of the light ends (<T_65) in the HCK reactor is observed for both cases. The rapid completion of the fast exocyclic β-scission reactions, also known as "paring reaction", can explain the rapid formation iso-paraffins in this range [45, 57]. In the paring reaction the branches of the naphthenic rings are cracked following a β-scission mechanism after being isomerized (See Figure 9). Irrespective of the original position of the branches, the prior isomerization brings them in a favorable arrangement for fast exocyclic β-scission, i.e. the *(t,t)* variant.

Figure 10 shows the reactor content profile of di-naphthenes with a carbon number between C11-C20 (Figure 10a) and C21-C30 (Figure 10b) for VGO$_C$. C11-C14 di-naphthenes (DIN11-DIN14) increase and C15-C30 di-naphthenes decrease, with the C21-C30 di-naphthenes decreasing rapidly. This is an evidence of de-branching reactions taking place. Di-naphthenes with 15 or more carbon atoms possess long substituents and, hence, there is a high probability of the alkyl substituents being rearranged via "Type B" isomerization in a configuration that promotes the formation of a carbocation in tertiary position. Once this type of carbocation is formed, the isomerized branch easily undergoes the fast *(t,t)* or "Type A" β-scission, forming di-naphthenes with 11 to 14 carbon atoms [13, 45, 57]. A similar behavior is also observed with mono-, di-, tri- and tetra-naphthenes. That also explains the high yield of iso-paraffins observed in Figure 7.
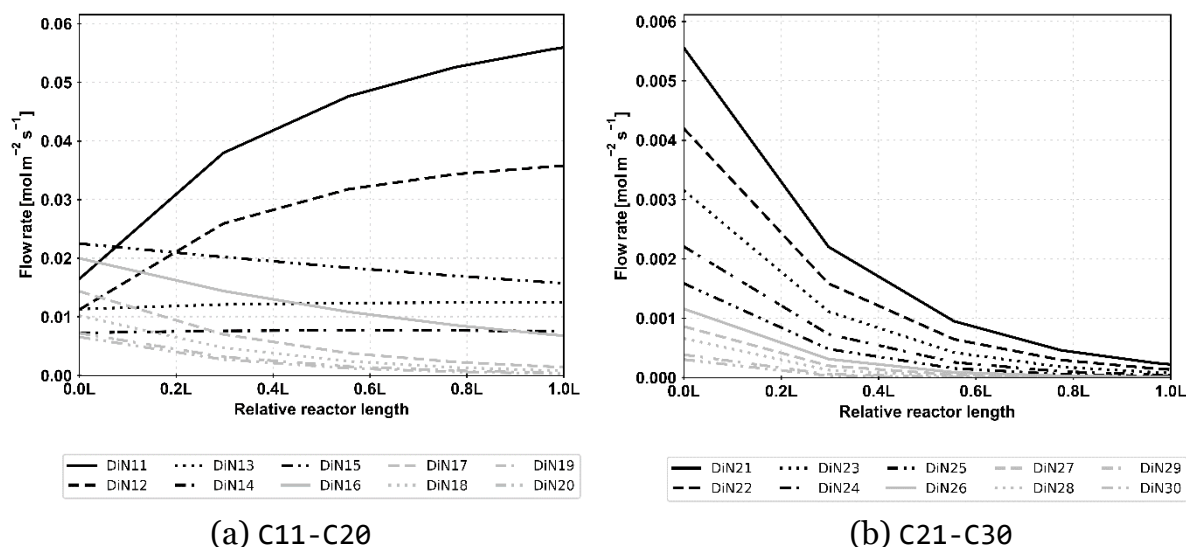
| (a) C11-C20 | (b) C21-C30 |

Figure 4. Di-naphthenes HCK reactor content profile for VGO_C

In case of CL a similar behavior is observed, with the only difference of a slightly increasing of C15 di-naphthenes formed through the same previously described mechanism. These results, together with the observed increase in paraffins, iso-paraffins and naphthenes in the range C4-C9 in Figure 8, in both configurations, results in a pronounced saturated (< T_150) cut, rich in paraffins and iso-paraffins.

3.1.2 Diesel (T_150_250)

The increase of the T_150_250 cut observed for both scenarios in Figures 6b and 6d respectively can be explained as a consequence of the increase of tetra-ring naphthenic with 18 carbon atoms produced from the fast exocyclic β-scission of tetra-ring naphthenes with more than 18 carbon atoms. The naphthenes increase is also a consequence of the hydrogenation of aromatics, where the produced alkyl-substituted naphthenes subsequently undergo the already described exocyclic β-scission or 'paring' reaction.

The increase in the fraction of paraffins, iso-paraffins and naphthenes observed in the range C10-C21 (~T150-T250 cut) for the two investigated feeds, shows a T_150_250 fraction rich in saturated compounds.

3.1.3 Light Vacuum Gas Oil (LVGO) (T_250_375)

Figure 6b show an slight decrease in the T_250_375 cut when processing VGO_C while Figure 6d shows a slight increase in the same cut when processing CL. This behavior

can be explained with the aid of Figure 8. According to Figure 8f, in case of CL, the mass fraction of compounds with carbon number in the range `C21-C30` (`~T_250_375`) in the outlet stream is higher than in the feed. The same figure shows that these compounds are mainly iso-paraffins. The mechanism that produces these iso-paraffins starts with the hydrogenation to naphthenes of the high amount of heavy poly-aromatics present in the CL, as described in Figure 8b, followed by subsequent isomerization and debranching of alkyl substituents as explained previously. Endocyclic β-scission of these naphthenes, even if slow, also takes place due to the high amount of poly-naphthenes as feed to the HCK as shown in Figure 8d.

In case of VGO_C, the decrease of this cut is attributed to the high concentration of mono-aromatics in the `T_250_375` cut (`~C21-C30`), which means, aromatics with long alkyl branches. The already explained hydrogenation followed by isomerization and debranching, together with the low content of `C35+` compounds, promotes the conversion of this fraction to lighter ones decreasing its final yield.

3.1.4 Heavy Vacuum Gas Oil (HVGO) (`T_T375_540`) and Residue (`T_540_plus`)

The yield of heavier cuts generally decreases because of the high level of hydrogenation of the aromatics contained in this fraction. As observed in Figure 7 for both scenarios, the decrease of all aromatics and corresponding increase of naphthenic compounds reflect the effect of the fast hydrogenation reactions in all aromatics families [52]. The presence of tetra-aromatics in the CL, explains the formation of tetra-naphtenics, which does not occur with the VGO_C, because of the absence of this class of compounds in the feed due to its lower final boiling point.

From a global point of view, these results show that the volumetric increase of the `IBP-T250` fraction in the case of VGO_C is +8% while for the CL it amounts to even +15%. In addition, the volumetric increase in the `IBP-T65` fraction in the case of VGO_C is +4% while for the CL it amounts to +9%. From Figure 8 it can be observed that the main change in the CL occurs in the heaviest fractions. That behavior can be attributed, in principle, to the hydrogenation of the high content of poly-aromatics. Once the aromatics are saturated, the isomerization followed by exocyclic β-scision of branches in naphthenes takes place. This fast reaction, together with the contribution of the slow endocyclic β-scision apparently limits the opportunity of reaching higher levels of conversion in the lightest fractions at the given conditions.

3.2 *Case Study*: Combined effect of temperature and catalyst acidity on C3-C21 yields

In this *simulation* scenario different combinations of protonation enthalpy (ΔH_{prot}) and reaction temperatures for both reactors are evaluated using VGO_B as feedstock. The aim is to perform an analysis of the yields of compounds with carbon number in the range of C3-C21. This range was selected because it constitutes the potential steam cracker feed. Different simulations to cover the following range were made: temperature, $[T^{ref} - 40°C : T^{ref} + 30°C]$, and ΔH_{prot}, $[\Delta H_{prot}^{ref} - 15 \text{ kJ/mol} : \Delta H_{prot}^{ref} + 15 \text{ kJ/mol}]$.
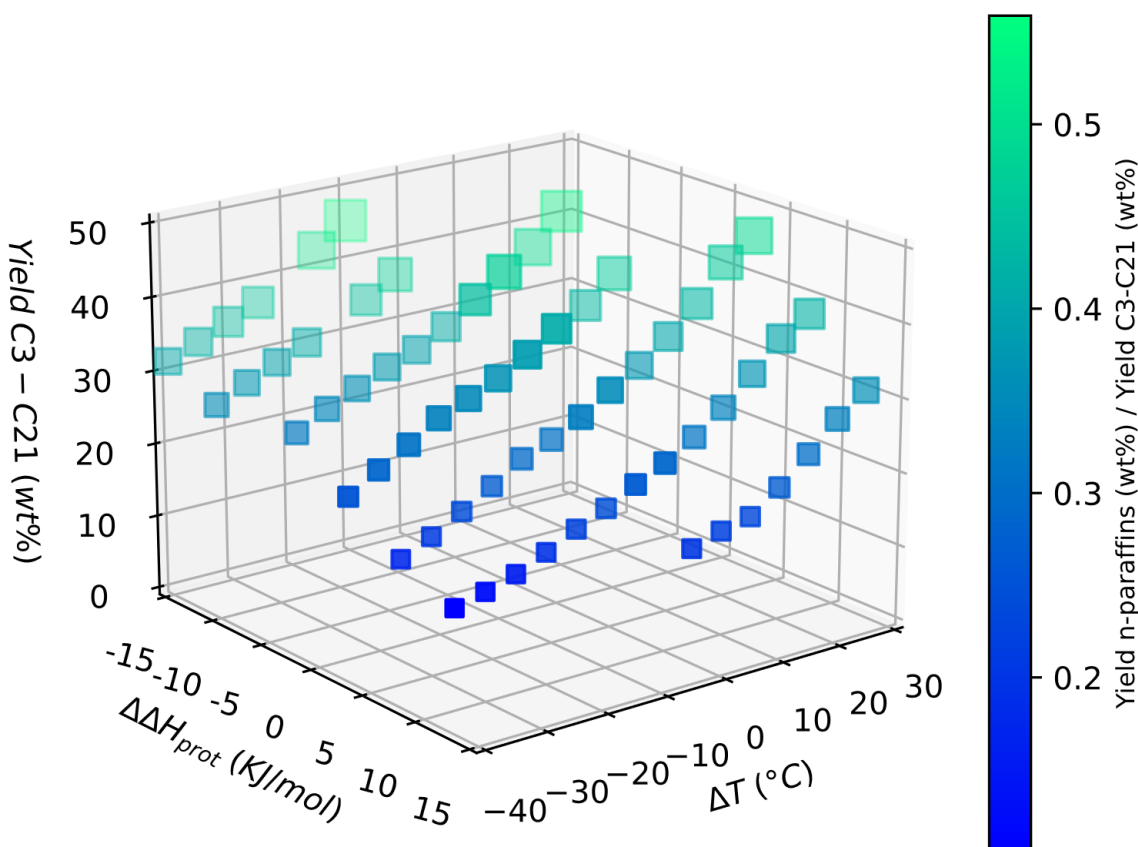
Figure 11. Yield to C3-C21 vs. $\Delta\Delta H_{prot}$ and $\Delta Temperature$. The color scale shows the ratio between n- and iso-paraffins and the size of the markers is proportional to the yield to paraffins in the range C3-C9

Figure 11 shows the results of the mentioned yields. In this figure the color scale represents the ratio between n-paraffins and iso-paraffins. These results show that at more severe conditions, i.e., higher acidity levels of the catalyst (more negative

510 $\Delta\Delta H_{prot}$) and higher temperature, not only the c3-c21 fraction yield increases, but also
511 the relative mass fraction of paraffins in this carbon range. An average rate of change
512 of +1.42 wt% in the yield of C3-C21 per kJ/mol decrease in the ΔH_{prot} of the catalyst
513 was obtained. Similarly, an average rate of change of +0.46 wt% in the yield of C3-C21
514 per °C increase in the operation temperature of both reactive sections was simulated.

515
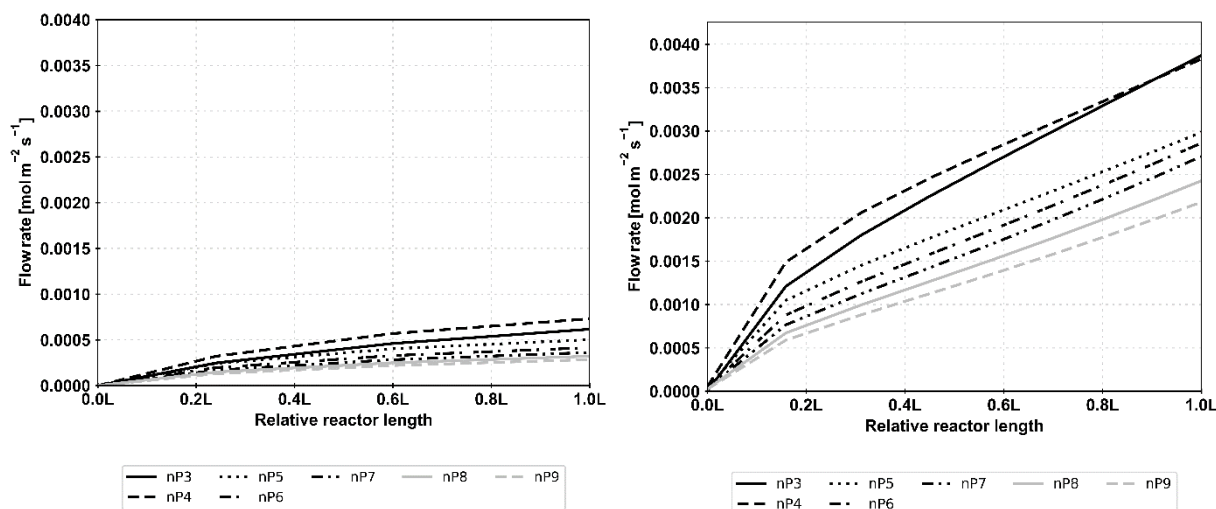
516

517 (a) $\Delta\Delta H_{prot} = -10 \ kJ/mol, \ \Delta T = -40°C$ (b) $\Delta\Delta H_{prot} = -5 \ kJ/mol, \ \Delta T = +10°C$

518
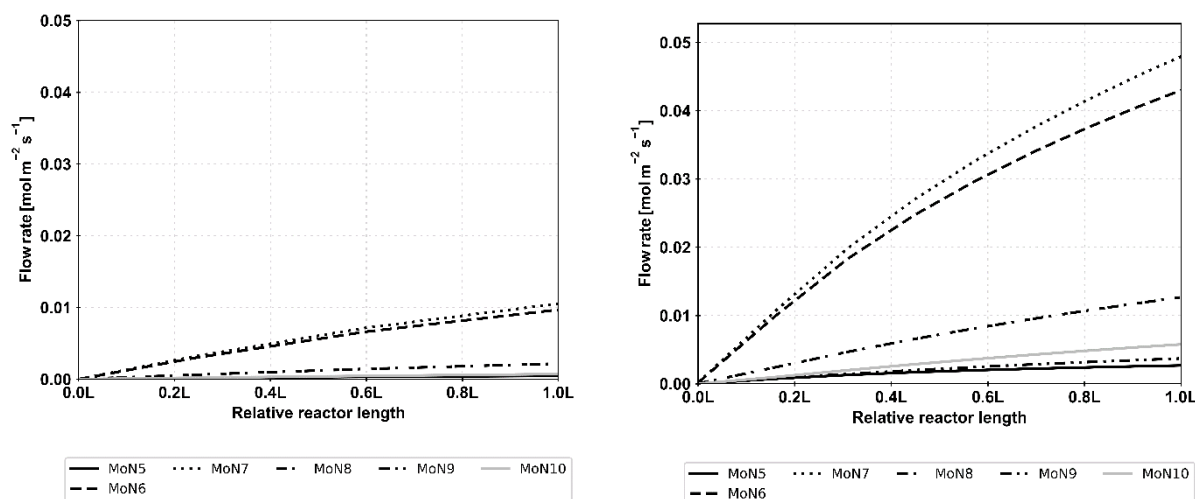
519

520 (c) $\Delta\Delta H_{prot} = -10 \ kJ/mol, \Delta T = -40°C$ (d) $\Delta\Delta H_{prot} = -5 \ kJ/mol, \Delta T = +10°C$

521 *Figure 5.* C3-C9 *n-Paraffins (a, b) and* C5-C10 *mono-naphthenes (c, d) molar flux profiles in the second reactor (HCK) for* VGO_B *at two different severity levels*

In the same figure, the size of the markers is proportional to the net yield of n-paraffins with carbon number between C3 and C9. It can be concluded that at more severe conditions also the yield of n-paraffins in the mentioned range increases. The molar flux profiles for paraffins and mono-naphthenes for two conditions with different severity, as shown in Figure 12, confirm that the molar flux of light paraffins increases with severity while the molar flux of mono-naphthenes increases to a lower extent.

These results indicate that, under these conditions, there is a particular increase of the endocyclic β-scission of mono-naphthenes promoting the production of compounds that constitute a convenient steam cracking feed. The endocyclic β-scission of mono-naphthenes is very well known as a slow reaction in hydrocracking [13, 29, 45]. The minimum orbital overlap of the β bond of the ring and the vacant p-orbital in the transition state make this reaction unlikely for 5-ring structures [57]. In the case of a 6-ring cycle the non-planarity of the molecule renders its occurrence somewhat more feasible, however, high severity conditions are still required.

Summarizing, with a change in the 'acidity strength' quantified as $\Delta\Delta H_{prot} = -5 \, kJ/mol$, together with a change in the operation temperature of $\Delta T = +10°C$, simulation results show that is possible to increase the yield of C3-C21 paraffins from 8.9% wt/wt to 19.6 % wt/wt. C3-C21 iso-paraffins increase from 8.5 % wt/wt to 17.9 % wt/wt, while C3-C21 n-paraffins increase from 0.4 % wt/wt to 1.7 % wt/wt. C3-C9 n-paraffins increase from 0.1% % wt/wt to 0.6% % wt/wt.

4   Conclusions

Crude Oil To Chemicals (COTC) is a novel concept that will be further deployed in the coming decades. Due to its flexibility to produce a diversity of light compounds, and the maturity of the process, hydroconversion is expected to play an important role in many COTC process configurations. Using an object-oriented simulation framework it was possible to relate bulk properties with a detailed molecular description of streams, which together with a fundamental kinetic model, allowed to obtain a quantitative insight in the hydroconversion of complex mixtures. A virgin VGO and a virgin full range light crude oil were chosen to describe key COTC process configurations where a downstream steam cracker allows to maximize the production of ethylene and

propylene. Paraffins in the C3-C21 range were considered to be a suitable feed for a steam cracker. Exocyclic β-scission of isomerized branches was demonstrated to be key in the iso-paraffins production in the desired range. n-Paraffins production requires the slow endocyclic β-scission of naphthenes. The simulation of different combinations of catalyst descriptors and process conditions allowed to conclude that a decrease in the acid strength of the catalyst quantified as $\Delta\Delta H_{prot} = -5\ kJ/mol$ combined with an increase in temperature of $\Delta T = +10°C$ is enough to double the C3-C21 mass paraffins yield. Under the same conditions the mass fraction of n-paraffins in the C3-C9 range increases up to 6 times. The endocyclic β-scission of mono-branched naphthenes with a linear alkyl group, which is promoted at higher severities, is the key reaction to produce n-paraffins in the C3-C9 range, a very convenient feed for steam crackers.

References

[1] "Petroleum & Other liquids. Refiney Yields," 2020.

[2] "BP Energy Outlook 2020".

[3] A. Corma, E. Corresa, Y. Mathieu, L. Sauvanaud, S. Al-Bogami, M. S. Al-Ghrami and A. Bourane, "Crude oil to chemicals: light olefins from crude oil," *Catalysis Science & Technology,* vol. 7, p. 12–46, 2017.

[4] R. J. Chang, "Crude oil to chemicals- Industry development and strategic implications," in *33nd Annual World Petrochemical Conference*, 2018.

[5] S. Gupta and D. Xu, "Business Trends: Crude-to-chemicals—An opportunity or threat?," 2019.

[6] S. A. Treese, P. R. Pujadó and D. S. J. J. (eds.), Handbook of Petroleum Processing, 2 ed., Springer International Publishing, 2015.

[7] "Process for production of hydrocarbon chemicals from crude oil". Patent US20130267745A1, 2013.

[8] K. Van Geem, "Single event microkinetic model for steam cracking of hydrocarbons," Ghent University, Faculty of Engineering, 2006.

[9] V. Kaiser, S. Barendreyt, P. J. Clymans and G. F. Froment, "Hydrotreated VGO is attractive as a feedstock for olefins," *Oil Gas J.; (United States),* vol. 82:44, 10 1984.

[10] J. Gary, Petroleum refining : technology and economics, Boca, Raton: CRC Press, 2007.

[11] J. G. Speight, Handbook of petroleum refining, Taylor & Francis;CRC Press, 2017.

[12] Fluid Catalytic Cracking Handbook, Elsevier, 2012.

[13] J. Thybaut and G. Marin, "Multiscale aspects in hydrocracking : from reaction mechanism over catalysts to kinetics and industrial application," *Advances in Catalysis,* vol. 59, p. 109–238, 2016.

[14] J. A. Scherzer and A. J. Gruia, Hydrocracking Science and Technology, vol. 69, Wiley, 1997, p. 1161–1162.

[15] J. Ancheyta, S. Sánchez and M. A. Rodrı́guez, "Kinetic modeling of hydrocracking of heavy oil fractions: A review," *Catalysis Today,* vol. 109, p. 76–92, 11 2005.

[16] G. F. Froment, "Single Event Kinetic Modeling of Complex Catalytic Processes," *Catalysis Reviews,* vol. 47, p. 83–124, 2 2005.

[17] J. Thybaut, C. L. Narasimhan and G. Marin, "Single Event MicroKinetics (SEMK) as a tool for catalyst and process design," in *Studies in Surface Science and Catalysis*, Gyeongju, 2006.

[18] M. Neurock, A. Nigam, D. Trauth and M. T. Klein, "Molecular representation of complex hydrocarbon feedstocks through efficient characterization and stochastic algorithms," *Chemical Engineering Science,* vol. 49, pp. 4153-4177, 1994.

[19] M. Klein, Molecular modeling in heavy hydrocarbon conversions, Boca Raton: CRC/Taylor & Francis, 2006.

[20] D. Hudebine and J. J. Verstraete, "Molecular reconstruction of LCO gasoils from overall petroleum analyses," *Chemical Engineering Science,* vol. 59, p. 4755–4763, 11 2004.

[21] K. Van Geem, D. Hudebine, M.-F. Reyniers, F. Wahl, J. J. Verstraete and G. Marin, "Molecular reconstruction of naphtha steam cracking feedstocks based on commercial indices," *Computers & Chemical Engineering,* vol. 31, p. 1020–1034, 2007.

[22] S. Pyl, K. Van Geem, M.-F. Reyniers and G. Marin, "Molecular reconstruction of complex hydrocarbon mixtures: an application of principal component analysis," *AICHE Journal,* vol. 56, p. 3174–3188, 2010.

[23] C. E. Shannon, "A mathematical theory of communication," *The Bell System Technical Journal,* vol. 27, pp. 379-423, 1948.

[24] G. G. Martens and G. B. Marin, "Kinetics for hydrocracking based on structural classes: Model development and application," *AIChE Journal,* vol. 47, pp. 1607-1622, 2001.

[25] M. R. Riazi, Characterization and properties of petroleum fractions, West, Conshohocken: ASTM International, 2005.

[26] S. Pyl, Z. Hou, K. Van Geem, M.-F. Reyniers, G. Marin and M. T. Klein, "Modeling the composition of crude oil fractions using constrained homologous series," *Industrial & Engineering Chemistry Research,* vol. 50, p. 10850–10858, 2011.

[27] T. Dijkmans, S. Pyl, C. Schietekat, K. Van Geem and G. Marin, "Detailed molecular compositions of heavy oil fractions by comprehensive two-dimensional gas chromatographic analysis," in *PetroleumPhase 2011*, London, 2011.

[28] A. Alvarez, L. C. Castañeda and J. Ancheyta, "On the application of petroleum feedstock modeling techniques for developing molecule-based models of

hydrocarbon conversion processes," *Catalysis Today,* Vols. 220-222, p. 198–207, 3 2014.

[29] A. Alvarez-Majmutov, J. Chen and R. Gieleciak, "Molecular-Level Modeling and Simulation of Vacuum Gas Oil Hydrocracking," *Energy & Fuels,* vol. 30, p. 138–148, 12 2015.

[30] P. Agarwal, M. Sahasrabudhe, S. Khandalkar, C. Saravanan and M. T. Klein, "Molecular-Level Kinetic Modeling of a Real Vacuum Gas Oil Hydroprocessing Refinery System," *Energy & Fuels,* vol. 33, p. 10143–10158, 9 2019.

[31] M. A. Baltanas, H. Vansina and G. F. Froment, "Hydroisomerization and hydrocracking. 5. Kinetic analysis of rate data for n-octane," *Industrial & Engineering Chemistry Product Research and Development,* vol. 22, p. 531–539, 12 1983.

[32] M. A. Baltanas and G. F. Froment, "Computer generation of reaction networks and calculation of product distributions in the hydroisomerization and hydrocracking of paraffins on Pt-containing bifunctional catalysts," *Computers & Chemical Engineering,* vol. 9, p. 71–81, 1 1985.

[33] P. J. Clymans and G. F. Froment, "Computer-generation of reaction paths and rate equations in the thermal cracking of normal and branched paraffins," *Computers & Chemical Engineering,* vol. 8, p. 137–142, 1 1984.

[34] L. P. Hillewaert, J. L. Dierickx and G. F. Froment, "Computer generation of reaction schemes and rate equations for thermal cracking," *AIChE Journal,* vol. 34, p. 17–24, 1 1988.

[35] M. A. Baltanas, K. K. Van Raemdonck, S. R. Mohedas and G. F. Froment, "Fundamental kinetic modeling of hydroisomerization and hydrocracking on noble metal-loaded faujasites. 1. Rate parameters for hydroisomerization," *Ind Eng Chem Res,* vol. 28, 1989/07/01.

[36] E. Vynckier and G. F. Froment, "Modeling of the kinetics of complex processes based upon elementary steps," in *Kinetic and Thermodynamic Lumping of Multicomponent Mixtures*, Elsevier, 1991, p. 131–161.

[37] W. Feng, E. Vynckier and G. F. Froment, "Single event kinetics of catalytic cracking," *Industrial & Engineering Chemistry Research,* vol. 32, p. 2997–3005, 12 1993.

[38] G. D. Svoboda, E. Vynckier, B. Debrabandere and G. F. Froment, "Single-Event Rate Parameters for Paraffin Hydrocracking on a Pt/US-Y Zeolite," *Industrial & Engineering Chemistry Research,* vol. 34, p. 3793–3800, 11 1995.

[39] J. W. Thybaut, G. B. Marin, G. V. Baron, P. A. Jacobs and J. A. Martens, "Alkene Protonation Enthalpy Determination from Fundamental Kinetic Modeling of Alkane Hydroconversion on Pt/H–(US)Y-Zeolite," *Journal of Catalysis,* vol. 202, p. 324–339, 9 2001.

[40] J. Thybaut, C. S. L. Narasimhan and G. Marin, "Bridging the gap between liquid and vapor phase hydrocracking," *Catalysis Today,* vol. 111, p. 94–102, 2006.

[41] C. S. L. Narasimhan, J. W. Thybaut, G. B. Marin, P. A. Jacobs, J. A. Martens, J. F. Denayer and G. V. Baron, "Kinetic modeling of pore mouth catalysis in the hydroconversion of n-octane on Pt-H-ZSM-22," *Journal of Catalysis,* vol. 220, p. 399–413, 12 2003.

[42] J. Thybaut and G. Marin, *Kinetic modeling of the conversion of complex hydrocarbon feedstocks by acid catalysts,* vol. 26, WILEY-V C H VERLAG GMBH, 2003, p. 509–514.

[43] J. Thybaut, C. S. L. Narasinham, J. F. Denayer, G. V. Baron, P. A. Jacobs, J. A. Martens and G. Marin, "Acid-metal balance of a hydrocracking catalyst: Ideal versus nonideal behavior," *Industrial & Engineering Chemistry Research,* vol. 44, p. 5159–5169, 2005.

[44] P. J. Becker, N. Serrand, B. Celse, D. Guillaume and H. Dulot, "Comparing hydrocracking models: Continuous lumping vs. single events," *Fuel,* vol. 165, p. 306–315, 2 2016.

[45] P. J. Becker, N. Serrand, B. Celse, D. Guillaume and H. Dulot, "A single events microkinetic model for hydrocracking of vacuum gas oil," *Computers & Chemical Engineering,* vol. 98, p. 70–79, 3 2017.

[46] I. R. Choudhury, J. Thybaut, P. Balasubramanian, J. F. M. Denayer, J. A. Martens and G. Marin, "Synergy between shape selective and non-shape selective bifunctional zeolites modelled via the Single-Event MicroKinetic (SEMK) methodology," *Chemical Engineering Science,* vol. 65, p. 174–178, 2010.

[47] I. R. Choudhury, K. Hayasaka, J. W. Thybaut, C. S. L. Narasimhan, J. F. Denayer, J. A. Martens and G. B. Marin, "Pt/H-ZSM-22 hydroisomerization catalysts optimization guided by Single-Event MicroKinetic modeling," *Journal of Catalysis,* vol. 290, pp. 165-176, 2012.

[48] N. V. Dewachtere, F. Santaella and G. F. Froment, "Application of a single-event kinetic model in the simulation of an industrial riser reactor for the catalytic cracking of vacuum gas oil," *Chemical Engineering Science,* vol. 54, p. 3653–3660, 7 1999.

[49] L. P. de Oliveira, D. Hudebine, D. Guillaume and J. J. Verstraete, "A Review of Kinetic Modeling Methodologies for Complex Processes," *Oil & Gas Science and Technology – Revue d'IFP Energies nouvelles,* vol. 71, p. 45, 5 2016.

[50] J. W. Thybaut, M. Saeys and G. B. Marin, "Hydrogenation kinetics of toluene on Pt/ZSM-22," *Chemical Engineering Journal,* vol. 90, p. 117–129, 11 2002.

[51] M. Saeys, J. Thybaut, M. Neurock and G. Marin, "Kinetic models for catalytic reactions from first principles: benzene hydrogenation," *Molecular Physics,* vol. 102, p. 267–272, 2004.

[52] J. W. Thybaut and G. B. Marin, "Single-Event MicroKinetics: Catalyst design for complex reaction networks," *Journal of Catalysis,* vol. 308, p. 352–362, 12 2013.

[53] J. Chen and R. A. Adomaitis, "An object-oriented framework for modular chemical process simulation with semiconductor processing applications," *Computers & Chemical Engineering,* vol. 30, p. 1354–1380, 7 2006.

[54] R. Waschler, O. Angeles-Palacios, M. Ginkel and A. Kienle, "Object-oriented modelling of large-scale chemical engineering processes with ProMoT," *Mathematical and Computer Modelling of Dynamical Systems,* vol. 12, p. 5–18, 2 2006.

[55] G. V. Varma, "Development of a process simulator using object oriented programming: Information modeling and program structure".

[56] G. VanRossum, The Python language reference, Hampton, NHRedwood City, Calif: Python Software FoundationSoHo Books, 2010.

[57] J. Weitkamp, "Catalytic Hydrocracking-Mechanisms and Versatility of the Process," *ChemCatChem,* vol. 4, p. 292–306, 2 2012.

567

568

569

570

List of Figures

Hydrocracking of complex mixtures: From bulk properties, over fundamental kinetics to detailed product composition

César G. Pernalete. P., Javier Ibáñez, Pedro S. F. Mendes, Kevin M. Van Geem, Joris W. Thybaut